Elastic electron scattering and the nuclear magnetization distribution*

J. F. Prewitt
Dikewood Corporation, Albuquerque, New Mexico 87106

L. E. Wright
Ohio University, Athens, Ohio 45701
(Received 21 December 1973)

An analysis of elastic electron scattering from the nuclear charge and magnetization distributions is carried out with phase-shift analysis and distorted-wave Born approximation, respectively. We find that magnetic electron scattering should be measurable from medium and heavy odd-A nuclei at normal scattering angles in addition to 180°. In particular, the scattering from the maximally allowed magnetic multipole distribution should be easily observed.

[NUCLEAR REACTIONS ^{27}Al, ^{51}V, ^{209}Bi elastic e^- scattering from magnetic moments odd-A nuclei calculated (phase shift and DWBA).]

INTRODUCTION

The interaction involved in the scattering of electrons from nuclei is electromagnetic in nature and thus only those aspects of nuclear structure contributing to the role of the nucleus as a source of the electromagnetic field are amenable to measurement by electron scattering. On the other hand, the electromagnetic interaction is well understood theoretically and thus permits the unambiguous examination of the nuclear charge and current distributions. Furthermore, if we restrict our attention to elastic electron scattering, the nucleus can be characterized by *static* electric and magnetic moment distributions since no energy is emitted or absorbed by the nucleus and the spatial dependence of these distributions can be extracted by analysis of electron scattering. Single-particle models of the nucleus predict relatively small nuclear magnetic multipole moments due to the pairing of the nucleon spins, thus predicting that magnetic moments are essentially due to single unpaired nucleons. This minimization of the number of nucleons contributing to the magnetic moments together with the fact that all the charge in the nucleus is positive (and a scalar), result in the domination of the electron-nucleus interaction by the electron-charge interaction. This result has been used extensively to study the nuclear ground-state charge distribution without being concerned with the nuclear magnetization distribution and consequently the nuclear charge distribution is much better known than the magnetization distribution. In this paper, we will be concerned with methods of extracting the nuclear magnetization distribution from elastic electron-nuclear scattering, particularly for the heavier nuclei.

In some ways, the nuclear magnetization distribution is more interesting than the nuclear charge distribution. By inverting the argument presented above, one sees that within a single-particle model the magnetization distribution arises from a single nucleon in the nucleus rather than a sum over all the protons, thus containing considerably more detail about the structure of the nucleus. Furthermore, the single nucleon can be a neutron which contributes little if anything to charge scattering and whose distribution in the nucleus is not well known experimentally and is of considerable interest theoretically. The magnetization distribution of isobars with either a single neutron or a single proton outside spin-zero cores should be quite interesting and may shed additional light on the question of the relative size of neutron and proton radii of nuclei.

The analysis of elastic electron scattering from the nuclear charge and current distributions is straightforward in the plane-wave Born approximation (PWBA), and has been successfully used to extract magnetic dipole, and in some cases, octopole moments in light odd-A nuclei[1,2] and to investigate the information obtainable from magnetic scattering.[3] A rather complete discussion of the investigation of magnetic properties of the nucleus using the Born approximation is given by Uberall.[4] As is well known, however, the plane-wave Born approximation fails for heavier nuclei, but since the PWBA does furnish a qualitative guide of what to expect experimentally and is a useful pedagogic framework we will include the PWBA results in our discussion. We only note here that most elec-

tron scattering experiments done to extract magnetic properties of nuclei have been done at 180° using the technique developed by Peterson and Barber.[5]

In order to obtain quantitative results from elastic electron scattering from medium and heavy nuclei, it is necessary to include the Coulomb distortion arising from the nuclear charge distribution in the incoming and outgoing electron wave functions. This can be done by solving the Dirac equation in the presence of a spherically symmetric Coulomb potential arising from the spherically symmetric portion of the nuclear charge distribution by phase-shift analysis. The remainder of the electron-nucleus interaction (i.e., the scattering of the electrons by the higher electric and the magnetic multipole moments) can be treated to first order in α, the fine-structure constant, by perturbation theory. One can visualize this as a Coulomb-distorted electron wave exchanging one virtual photon (which for elastic scattering has zero energy, but carries momentum) with the electric and magnetic multipole moment distributions of the nucleus. For the case of inelastic electron scattering we would refer to this by the term distorted-wave Born approximation (DWBA). We expect first-order perturbation theory to be quite accurate for the scattering from the electric and magnetic multipole moments since the interaction falls off as $1/r^2$ or greater and only few nucleons contribute to the higher electric and magnetic multipole moments.

In the theory section we give the details of the phase-shift analysis, which is quite standard except we do not make the so-called high-energy approximation ($m_0/E \to 0$) since it is not valid at 180°. We also give the details of the DWBA calculation as applied to elastic scattering, and show that for the special case of elastic scattering one of the major problems of DWBA calculations, the numerical evaluation of radial matrix elements over a large range, can be avoided. This is an important point for computational considerations since in DWBA, unlike the PWBA case, the experimentally measured form factors cannot be inverted to obtain the charge and current distributions, thereby requiring a parametrization of the charge and current distributions and doing repeated DWBA analysis with different values of the parameters. Furthermore, extended numerical integration leads to lack of precision due to cumulative round-off errors.

Finally, using simple parametrizations and models for the charge and current distributions we examine the possibility of extracting the magnetization distribution of medium and heavy nuclei from elastic electron scattering.

THEORY

Phase-shift analysis

As noted in the Introduction, the spherically symmetric Coulomb potential $V(r)$ is included in the unperturbed Hamiltonian describing the electron. Thus we must solve the Dirac equation for electrons of energy E in the presence of the Coulomb field. In polar form the Dirac-Coulomb equation is

$$\left[-i\alpha_r\left(\frac{\partial}{\partial r}+\frac{1}{r}-\frac{\beta K}{r}\right)+V(r)+\beta m_0\right]\phi_m(\vec{r})=E\phi_m(\vec{r}), \tag{1}$$

where the Dirac operator K is given by $K\equiv\beta(\vec{\sigma}\cdot\vec{L}+1)$ and m is electron spin projection. It is convenient to expand $\phi_m(\vec{r})$ in free-particle spinors

$$\phi_m(\vec{r})=4\pi\left(\frac{E+m_0}{2EV}\right)^{1/2}\sum_{\kappa\mu}e^{i\delta_\kappa}i^l C_{\mu-m\ m}^{\ l\ 1/2\ j}\times Y_l^{\mu-m*}(\hat{p}_i)\phi_\kappa^\mu(\vec{r}), \tag{2}$$

where κ is the eigenvalue of the operator K and j is the total angular momentum and l is the orbital angular momentum corresponding to the κth partial wave. They are given explicitly by

$$j=|\kappa|-\tfrac{1}{2},\quad l=\begin{cases}\kappa & \kappa>0\\ -\kappa-1 & \kappa<0\end{cases}.$$

The wave functions are normalized in a large volume V which will henceforth be set to 1. The four-component functions $\phi_\kappa^\mu(\vec{r})$ can be separated into radial and spin-angle parts by writing

$$\phi_\kappa^\mu(\vec{r})=\begin{pmatrix} g_\kappa(r)\,\chi_\kappa^\mu(\hat{r})\\ if_\kappa(r)\,\chi_{-\kappa}^\mu(\hat{r})\end{pmatrix}, \tag{3}$$

where

$$\chi_\kappa^\mu(\hat{r})=\sum_{m'}C_{m'\ \mu-m'\ \mu}^{l\ 1/2\ j}\,Y_l^{m'}(\hat{r})\chi_{\mu-m'}.$$

The radial functions $f_\kappa(r)$ and $g_\kappa(r)$ satisfy the following coupled first-order differential equations:

$$\frac{d}{dr}\begin{pmatrix}f_\kappa(r)\\ g_\kappa(r)\end{pmatrix}=p\begin{pmatrix}0 & -[E-m_0-V(r)]\\ [E+m_0-V(r)] & 0\end{pmatrix}\times\begin{pmatrix}f_\kappa(r)\\ g_\kappa(r)\end{pmatrix}+\frac{1}{r}\begin{pmatrix}\kappa-1 & 0\\ 0 & -\kappa-1\end{pmatrix}\begin{pmatrix}f_\kappa(r)\\ g_\kappa(r)\end{pmatrix}, \tag{4}$$

where p is the magnitude of the electron momentum.

The elastic scattering amplitude for an electron with initial spin m is given in terms of the phase shifts δ_κ appearing in Eq. (2) by[4]

$$a_m(\hat{r}) = \frac{-2\pi i}{p} \sum_{\kappa\mu} (e^{2i\delta_\kappa} - 1) C^{l}_{\mu-m}{}^{1/2}_{m}{}^{j}_{\mu} Y_l^{\mu-m*}(\hat{p}_i) \chi_\kappa^\mu(\hat{r}), \tag{5}$$

where $\hat{p}_i$ is the direction of the incident electron momentum and $\hat{r}$ is the direction of the outgoing scattered electron. Choosing $\hat{p}_i$ to be the z axis and using the explicit form of $\chi_\kappa^\mu(\hat{r})$ from Eq. (3) we can write the scattering amplitude as

$$a_m(\hat{r}) = f(\theta)\chi_m + 2m g(\theta) e^{2mi\phi} \chi_{-m}, \quad m = \pm\tfrac{1}{2}, \tag{6}$$

where the non-spin-flip amplitude $f(\theta)$ is given by

$$f(\theta) = \frac{1}{2ip} \sum_{\kappa>0} \kappa [e^{2i\delta_\kappa} P_\kappa(\cos\theta) + e^{2i\delta_{-\kappa}} P_{\kappa-1}(\cos\theta)]$$

and the spin-flip amplitude $g(\theta)$ is given by

$$g(\theta) = \frac{1}{2ip} \sum_{\kappa>0} [e^{2i\delta_\kappa} P_\kappa{}^1(\cos\theta) - e^{2i\delta_{-\kappa}} P_{\kappa-1}{}^1(\cos\theta)].$$

For convenience we introduce $\Delta_\kappa \equiv \delta_{-\kappa} - \delta_\kappa$ and use the relations

$$P_{\kappa-1}{}^1(\cos\theta) = -\kappa[P_\kappa(\cos\theta) - \cos\theta P_{\kappa-1}(\cos\theta)]/\sin\theta$$

and

$$P_\kappa{}^1(\cos\theta) = -\kappa[\cos\theta P_\kappa(\cos\theta) - P_{\kappa-1}(\cos\theta)]/\sin\theta$$

to write

$$f(\theta) = \frac{1}{2ip} \sum_{\kappa>0} \kappa e^{2i\delta_\kappa} [P_\kappa(\cos\theta) + e^{2i\Delta_\kappa} P_{\kappa-1}(\cos\theta)], \tag{7}$$

$$g(\theta) = \frac{1}{\sin\theta} \left\{ \frac{1}{2ip} \sum_{\kappa>0} \kappa e^{2i\delta_\kappa} (1 + e^{2i\Delta_\kappa}) \times [P_\kappa(\cos\theta) + P_{\kappa-1}(\cos\theta)] - (1+\cos\theta) f(\theta) \right\}. \tag{8}$$

Note that the spin-flip amplitude $g(\theta)$ vanishes at $\theta = 180°$. Furthermore, if the high-energy limit is taken ($m_0/E \to 0$), it can be shown that $\delta_\kappa = \delta_{-\kappa}$ and $f(\theta)$ also vanishes at 180°. The physical reason for this is that in the high-energy limit the electron helicity $\vec{\sigma}\cdot\vec{p}$ is a good quantum number and exact 180° scattering would require a spin-flip amplitude which charge scattering cannot furnish.

For values of the electron coordinate r outside the nuclear charge distribution (taken to be zero beyond some radius R), the Coulomb potential becomes $V(r) = -\alpha Z/r$ and thus the radial functions $f_\kappa(r)$ and $g_\kappa(r)$ can be expressed as linear combinations of the point regular and irregular Coulomb wave functions

$$\begin{aligned} f_\kappa(r) &= A_\kappa f_\kappa^{\mathrm{CR}}(r) + B_\kappa f_\kappa^{\mathrm{CI}}(r), \\ g_\kappa(r) &= A_\kappa g_\kappa^{\mathrm{CR}}(r) + B_\kappa g_\kappa^{\mathrm{CI}}(r), \end{aligned} \qquad r \geq R. \tag{9}$$

The superscript C denotes point Coulomb, while R and I refer to the regular and irregular solutions, respectively. Analytic expressions for and asymptotic forms of these point Coulomb functions are given in the Appendix.

The normalized asymptotic forms of $f_\kappa(r)$ and $g_\kappa(r)$ are

$$\begin{aligned} f_\kappa(r) &\to -\left(\frac{E-m_0}{E+m_0}\right)^{1/2} \times \frac{\sin[pr + y\ln 2pr - \frac{1}{2}(l+1)\pi + \delta_\kappa]}{pr}, \\ g_\kappa(r) &\to \frac{\cos[pr + y\ln 2pr - \frac{1}{2}(l+1)\pi + \delta_\kappa]}{pr}, \end{aligned} \tag{10}$$

where $y = \alpha ZE/p$ and δ_κ are the phase shifts appearing in Eqs. (7) and (8) for the scattering amplitudes. It is useful to write $\delta_\kappa = \delta_\kappa^{\mathrm{R}} + \bar{\delta}_\kappa$ where $\delta_\kappa^{\mathrm{R}}$ are the phase shifts of the regular point Coulomb wave functions and $\bar{\delta}_\kappa$ are the additional phases arising from the finite extent of the nuclear charge distribution, and thus contain all the information about the spherically symmetric charge distribution.

Using the asymptotic forms of the point solutions given in the Appendix and Eq. (10) above we find

$$\bar{\delta}_\kappa = \arctan\left(\frac{\sin\theta_\kappa}{A_\kappa/B_\kappa + \cos\theta_\kappa}\right), \tag{11}$$

where $\theta_\kappa \equiv \delta_\kappa^{\mathrm{I}} - \delta_\kappa^{\mathrm{R}}$. The regular and irregular Coulomb phase shifts are given explicitly by

$$\delta_\kappa^{\mathrm{R}} = -\frac{\pi}{2}\frac{(1+S_\kappa)}{2} - \tfrac{1}{2}\arctan\frac{y(\kappa+\gamma m_0/E)}{\kappa\gamma - y^2 m_0/E} - \frac{\pi}{2}\gamma - \arg\Gamma(\gamma+iy) + \frac{l+1}{2}\pi, \tag{12}$$

where $S_\kappa = \kappa/|\kappa|$, $\gamma = (\kappa^2 - \alpha^2 Z^2)$, and $\delta_\kappa^{\mathrm{I}} = \delta_\kappa^{\mathrm{R}}(-\gamma)$. Using these expressions we obtain

$$\theta_\kappa = -\pi(|\kappa| - \gamma) - \arctan\{\coth\pi y \times [\tan\pi(|\kappa| - \gamma)]\} + \tfrac{1}{2}\pi \tag{13}$$

which is valid in general and not only in the high-energy limit as implied in Ref. 4.

The calculational procedure is to integrate numerically the radial equations [Eq. (4)] from the origin to the nuclear cutoff radius R and compare the values of $f_\kappa(r)$ and $g_\kappa(r)$ to the point Coulomb wave functions and extract the phase shifts as outlined above. The phases are inserted into Eqs. (7) and (8) and the series reduction method of Yennie, Ravenhall, and Wilson[6] is used to speed convergence of the partial-wave series for the amplitudes. This procedure works quite well and enables us to calculate charge scattering all the way to 180°. We note the obvious point that all the charge scattering information is contained in the values of the electron wave functions at the nuclear cutoff radius R.

Distorted-wave Born approximation

The interaction Hamiltonian for the electron in the presence of the static nuclear charge [excluding $\rho_0(r)$], current, and magnetization densities may be written to first order in α in the Coulomb gauge as

$$H_{\rm int} = -\alpha \left\{ \int [\rho'(\vec{r}_n)\phi_e(\vec{r}_n) - \vec{j}_0(\vec{r}_n)\cdot\vec{A}_e(\vec{r}_n) - \mu(\vec{r}_n)\cdot\vec{B}_e(\vec{r}_n)]\, d\tau_n \right\}, \tag{14}$$

where the scalar and vector potentials at the field point $\vec{r}_n$ due to the passing electron are given by

$$\phi_e(\vec{r}_n) = \int \frac{\rho_e(\vec{r}_e)}{|\vec{r}_n - \vec{r}_e|}\, d\tau_e \tag{15}$$

and

$$\vec{A}_e(\vec{r}_n) = \int \frac{\vec{I}\cdot\vec{j}_e(\vec{r}_e)}{|\vec{r}_n - \vec{r}_e|}\, d\tau_e . \tag{16}$$

The magnetic field $\vec{B}_e(\vec{r}_n) = \vec{\nabla}\times\vec{A}_e(\vec{r}_n)$, and the electron charge and current densities are given by

$$\rho_e(\vec{r}_e) = \langle\phi_f|\rho_e^{0\rho}|\phi_i\rangle = \phi_f^\dagger(\vec{r}_e)\phi_i(\vec{r}_e),$$

$$\vec{j}_e(\vec{r}_e) = \langle\phi_f|\vec{j}_e^{0\rho}|\phi_i\rangle = \phi_f^\dagger(\vec{r}_e)\vec{\alpha}\phi_i(\vec{r}_e),$$

where the ϕ's are initial and final electron wave functions in the presence of the Coulomb field and are given explicitly in Eq. (2). The derivation of the scattering amplitude can be simplified by defining $\vec{j}_T(\vec{r}_n) = \vec{j}_0(\vec{r}_n) + \vec{\nabla}\times\vec{\mu}(\vec{r}_n)$ and using vector identities to write

$$H_{\rm int} = -\alpha \int [\rho'(\vec{r}_n)\phi_e(\vec{r}_n) - \vec{j}_T(\vec{r}_n)\cdot\vec{A}(\vec{r}_e)]\, d\tau_n , \tag{17}$$

where we have used the fact that the surface term vanishes at the origin and at infinity.

A multipole expansion of the scalar and vector potentials can be obtained by expanding $1/|\vec{r}_n - \vec{r}_e|$ and $\vec{I}/|\vec{r}_n - \vec{r}_e|$ in scalar and vector spherical harmonics, respectively:

$$\frac{1}{|\vec{r}_n - \vec{r}_e|} = \sum_{L,M} \frac{4\pi}{2L+1} r_<^L r_>^{-L-1} Y_L^M(\hat{r}_e) Y_L^{M*}(\hat{r}_n), \tag{18}$$

$$\frac{\vec{I}}{|\vec{r}_n - \vec{r}_e|} = \sum_{J,L,M} \frac{4\pi}{2L+1} r_<^L r_>^{-L-1} \vec{Y}_{J,L}^M(\hat{r}_e) \vec{Y}_{J,L}^{M*}(\hat{r}_n).$$

Furthermore, due to parity conservation and time-reversal invariance only even electric multipoles and odd magnetic multipoles can contribute to elastic electron scattering,[4] and we can write

$$\phi_e(\vec{r}_n) = \sum_{\substack{L,M \\ L=\text{even}}} \frac{4\pi}{2L+1} \int r_<^L r_>^{-L-1} \rho_e(\hat{r}_e) Y_L^M(\hat{r}_e)\, d\tau_e \times Y_L^{M*}(\hat{r}_n),$$

$$\vec{A}_e(\vec{r}_n) = \sum_{\substack{L,M \\ L=\text{odd}}} \frac{4\pi}{2L+1} \int r_<^L r_>^{-L-1} \vec{j}_e(\vec{r}_e)\cdot\vec{Y}_{L,L}^M(\hat{r}_e)\, d\tau_e \times \vec{Y}_{L,L}^{M*}(\hat{r}_n).$$

Consequently, the static nuclear charge and current distributions can be expanded as

$$\rho'(\vec{r}_n) = \sum_{\substack{L,M \\ L=\text{even}\neq 0}} \frac{(-1)^{L-M}}{\hat{J}} C_{-M\,M_i\,M_f}^{L\,J\,J} \rho_L(r_n) Y_L^M(\hat{r}_n), \tag{20}$$

$$\vec{j}(\vec{r}_n) = \sum_{\substack{L,M \\ L=\text{odd}}} \frac{(-1)^{L-M}}{\hat{J}} C_{-M\,M_i\,M_f}^{L\,J\,J} j_{L,L}(r_n) \vec{Y}_{L,L}^M(\hat{r}_n), \tag{21}$$

where (J,M_i) and (J,M_f) are the initial and final nuclear spins and projections, and $\hat{J} = (2J+1)^{1/2}$. Similar considerations permit the intrinsic magnetization $\vec{\mu}$ to be expanded as

$$\vec{\mu}(\vec{r}_n) = \sum_{\substack{L,M \\ L=\text{odd}}} \frac{(-1)^{L-M}}{\hat{J}} C_{-M\,M_i\,M_f}^{L\,J\,J} [\mu_{L,L+1}(r_n)\vec{Y}_{L,L+1}^M(\hat{r}_n) + \mu_{L,L-1}(r_n)\vec{Y}_{L,L-1}^M(\hat{r}_n)].$$

Choosing the initial electron momentum $\vec{p}_i = p_i\hat{z}$ to define the z axis, and substituting all the multipole

and partial wave expansions above into Eq. (17) and performing the angular integrals over the nuclear and electron coordinates, the matrix elements of $H_{\rm int}$ between initial and final spin states are given by

$$\langle m'M_f|H_{\rm int}|mM_i\rangle_{LM}=8\pi^2\frac{E+m_0}{E}\alpha\frac{(-1)^{L-M}}{\hat{J}\hat{L}}C^{\ L\ \ J\ \ J}_{-M\ M_i\ M_f}$$
$$\times\sum_{\kappa\kappa'}(-1)^{j'+L+l+\frac{1}{2}}(2l+1)(2j+1)^{1/2}e^{i(\delta_\kappa+\delta_{\kappa'})}i^{l-l'}C^{l\ \ \frac{1}{2}\ \ j}_{0\ \ m\ \ m}C^{l'\ \ \frac{1}{2}\ \ j'}_{m+M-m'\ \ m'\ \ m+M}C^{j\ \ L\ \ j'}_{m\ \ M\ \ m+M}$$
$$\times\left[C^{l\ L\ l'}_{0\ 0\ 0}W(j'l'jl;\tfrac{1}{2}L)R^E(\kappa,L,\kappa')+\frac{i(\kappa+\kappa')}{[L(L+1)]^{1/2}}C^{l\ \ L\ \ \bar{l}'}_{0\ \ 0\ \ 0}W(j'\bar{l}'jl;\tfrac{1}{2}L)R^M(\kappa,L,\kappa')\right]Y^{m+M-m'}_{l'}(\hat{p}_f), \tag{22}$$

Where the radial integrals in this expression are defined by

$$R^E(\kappa,L,\kappa')=\int_0^\infty\int_0^\infty[f_\kappa(r_e)f_{\kappa'}(r_e)+g_\kappa(r_e)g_{\kappa'}(r_e)]r_<^L r_>^{-L-1}\rho_L(r_n)r_n^2r_e^2dr_e\,dr_n, \tag{23}$$

$$R^M(\kappa,L,\kappa')=\int_0^\infty\int_0^\infty[f_\kappa(r_e)g_{\kappa'}(r_e)+g_\kappa(r_e)f_{\kappa'}(r_e)]r_<^L r_>^{-L-1}j_{L,L}(r_n)r_n^2r_e^2dr_e\,dr_n. \tag{24}$$

The symbol $\bar{l}$ appearing in the magnetic contribution is to be interpreted as $\bar{l}\equiv l(-\kappa)$.

The magnetic radial integral of Eq. (24) can also be expressed in terms of the radial distributions of the orbital current and the spin magnetization distributions. Using $\vec{j}_T(\vec{r})=\vec{j}_0(\vec{r})+\vec{\nabla}\times\vec{\mu}(\vec{r})$ we obtain

$$j_{L,L}(r)=j^0_{L,L}(r)+\frac{i}{(2L+1)^{1/2}}\frac{d}{dr}[\sqrt{L}\,\mu_{L,L+1}(r)+(L+1)^{1/2}\mu_{L,L-1}(r)]$$
$$+\frac{1}{r}[\sqrt{L}\,(L+2)\mu_{L,L+1}(r)-(L+1)^{1/2}(L-1)\mu_{L,L-1}(r)]. \tag{25}$$

Substituting this expression in Eq. (24) and integrating the integral over the nuclear coordinate by parts the magnetic radial integral can be expressed as,

$$R^M(\kappa,L,\kappa')=\int_0^\infty[f_\kappa(r_e)g_{\kappa'}(r_e)+g_\kappa(r_e)f_{\kappa'}(r_e)]$$
$$\times\left\{\int_0^\infty\frac{r_<^L}{r_>^{L+1}}j^0_{L,L}(r_n)r_n^2dr_n+i(2L+1)^{1/2}\right.$$
$$\left.\times\left(\frac{-(L+1)^{1/2}}{r_e^{L+1}}\int_0^{r_e}r_n^{L+1}\mu_{L,L-1}(r_n)dr_n+\sqrt{L}\,r_e^L\int_{r_e}^\infty\frac{\mu_{L,L+1}(r_n)}{r_n^L}dr_n\right)\right\}r_e^2dr_e\,.$$

Note that only the $\vec{Y}_{L,L-1}$ component of the spin magnetization $\vec{\mu}$ contributes to the scattering when $r_e>r_n$ and that only the $\vec{Y}_{L,L+1}$ component contributes when $r_e<r_n$. Thus nonpenetrating orbits only scatter from the $\vec{Y}_{L,L-1}$ component of the spin magnetization.

Averaging the amplitude squared over initial spin states, summing over final spin states, multiplying by the density of final states, and dividing by the incident flux the contribution to the differential scattering cross section due to the scattering from a multipole moment of order L is

$$\left(\frac{d\sigma(\theta)}{d\Omega}\right)_L=\frac{E^2}{4\pi^2}\sum_{M,\,m'}\frac{1}{(2J+1)(2L+1)}|\langle f|H_{\rm int}|i\rangle_{LM}|^2. \tag{26}$$

The differential elastic scattering cross section from all electric and magnetic multipoles is

$$\frac{d\sigma(\theta)}{d\Omega}=\sum_L\left(\frac{d\sigma(\theta)}{d\Omega}\right)_L,$$

where all cross terms [including those with the spherically symmetric charge scattering amplitude of Eq. (6)] vanish due to the orthogonality of the vector coupling coefficients. The matrix element $\langle f|H_{\rm int}|i\rangle_{LM}$ in Eq. (26) is related to the one of Eq. (22) by

$$\langle m',M_f|H_{\rm int}|m,M_i\rangle_{LM}=\frac{(-1)^{L-M}}{\hat{J}}C^{\ L\ \ J\ \ J}_{-M\ M_i\ M_f}$$
$$\times\langle f|H_{\rm int}|i\rangle_{LM}.$$

In order to characterize the magnitude of the electron scattering from the nuclear moments, we define the electric and magnetic multipole moments in the stretched configuration as

$$Q_L = \left(\frac{4\pi}{2L+1}\right)^{1/2} \int r^L Y_L^{0*}(\hat{r}) \rho(\hat{r}) d\tau \tag{27}$$

and

$$M_L = i \left(\frac{4\pi L}{(L+1)(2L+1)}\right)^{1/2} \int r^L \vec{Y}^{0*}_{L,L}(\hat{r}) \cdot \vec{j}_T(\vec{r}) d\tau . \tag{28}$$

Recalling that $\vec{j}_T(\vec{r}) = j_0(\vec{r}) + \vec{\nabla} \times \vec{\mu}(\vec{r})$, the magnetic moments can be written as a sum of orbital and intrinsic magnetization terms:

$$M_L = (4\pi L)^{1/2} \left(\frac{i}{[(L+1)(2L+1)]^{1/2}} \int r^L \vec{Y}^{0*}_{LL} \cdot \vec{j}_0 d\tau + \int r^{L-1} \vec{Y}^{0*}_{L,L-1} \cdot \vec{\mu} d\tau \right), \tag{29}$$

where as noted above only the $\vec{Y}^0_{L,L-1}$ component of $\vec{\mu}$ contributes to the magnetic multipole moment.

As noted in the Introduction, the difficulty with calculating the scattering amplitude in distorted-wave Born approximation is the evaluation of the radial integrals which occur in the scattering amplitude. Consider the magnetic radial integral of Eq. (25) as an example. We can write it as

$$R^M(\kappa, L, \kappa') = \int_0^\infty \left[r_n^{-L-1} \int_0^{r_n} r_e^{L+2} (f_\kappa g_{\kappa'} + g_\kappa f_{\kappa'}) dr_e + r_n^L \times \int_{r_n}^\infty r_e^{-L+1} (f_\kappa g_{\kappa'} + g_\kappa f_{\kappa'}) dr_e \right] \times j_{L,L}(r_n) r_n^2 dr_n .$$

The integration over the electron coordinate r_e inside the nucleus must be done numerically since the electron wave functions f_κ and g_κ depend on the details of the nuclear charge distribution $\rho_0(r)$ and are in fact generated numerically. However, for values of $r_e \geq R$, where R is the nuclear cutoff radius, the electron wave functions are linear combinations of regular and irregular point Coulomb wave functions which are known analytically. With this point in mind, consider the integrals

$$I^i_{L-1}(R) \equiv R^{L-2} \int_R^\infty \frac{S^i_{\kappa\kappa'}(r_e)}{r_e^{L-1}} dr_e , \quad i = 1, 2 , \tag{30}$$

where

$$S^1_{\kappa\kappa'}(r_e) = \begin{pmatrix} \phi_\kappa(r_e) \phi_{\kappa'}(r_e) \\ \phi^*_\kappa(r_e) \phi^*_{\kappa'}(r_e) \end{pmatrix},$$

$$S^2_{\kappa\kappa'}(r_e) = \begin{pmatrix} \phi_\kappa(r_e) \phi^*_{\kappa'}(r_e) \\ \phi^*_\kappa(r_e) \phi_{\kappa'}(r_e) \end{pmatrix},$$

and

$$\phi_\kappa(r_e) = \frac{f_\kappa(r_e)}{(E-m_0)^{1/2}} - i \frac{g_\kappa(r_e)}{(E+m_0)^{1/2}} .$$

For $r_e \geq R$, the ϕ_κ satisfy the Dirac-Coulomb radial equations

$$\frac{d}{dr} \begin{pmatrix} \phi_\kappa(r) \\ \phi^*_\kappa(r) \end{pmatrix} = -ip\sigma_z \begin{pmatrix} \phi_\kappa(r) \\ \phi^*_\kappa(r) \end{pmatrix} + \frac{1}{r} \begin{pmatrix} -1-iy & \kappa+i\beta \\ \kappa-i\beta & -1+iy \end{pmatrix} \times \begin{pmatrix} \phi_\kappa(r) \\ \phi^*_\kappa(r) \end{pmatrix}, \tag{31}$$

where $\beta = \alpha Z m_0/p$ and $y = \alpha ZE/p$. The integrals of interest are given in terms of I^i_{L-1} by

$$\int_R^\infty \frac{f_\kappa g_{\kappa'} + g_\kappa f_{\kappa'}}{r_e^{L-1}} dr_e = \frac{-p}{R^{L-2}} \operatorname{Im}[I^1_{L-1}(R)]$$

and

$$\int_R^\infty \frac{f_\kappa f_{\kappa'} + g_\kappa g_{\kappa'}}{r_e^{L-1}} dr_e = \frac{1}{R^{L-2}} \operatorname{Re}[m_0 I^1_{L-1}(R) + E I^2_{L-1}(R)] .$$

Integrating the integrals I^i_{L-1} by parts and using Eq. (31) to eliminate the derivatives of the wave functions we obtain the following matrix equations:

$$I^1_{L-1}(r) = \frac{1}{2ipR} \left[\sigma_z S^1_{\kappa\kappa'}(R) + \frac{B}{(L+1)} S^2_{\kappa\kappa'}(R) + C_L I^1_L(R) \right],$$

$$I^2_{L-1}(R) = \frac{1}{L} [S^2_{\kappa\kappa'}(R) + D I^1_{L-1}(R)],$$

where the 2×2 matrices B, C_L, and D are given by

$$B = \begin{pmatrix} \kappa'+i\beta & \kappa+i\beta \\ -(\kappa-i\beta) & -(\kappa'-i\beta) \end{pmatrix}, \quad D = \begin{pmatrix} \kappa'-i\beta & \kappa+i\beta \\ \kappa-i\beta & \kappa'+i\beta \end{pmatrix},$$

and

$$C_L = \begin{pmatrix} -(L+1+2iy) + \dfrac{\kappa^2+\kappa'^2+2\beta^2}{L+1} & \dfrac{2(\kappa+i\beta)(\kappa'+i\beta)}{L+1} \\ \dfrac{-2(\kappa-i\beta)(\kappa'-i\beta)}{L+1} & (L+1-2iy) - \dfrac{\kappa^2+\kappa'^2+2\beta^2}{L+1} \end{pmatrix}.$$

We have expressed the desired integrals in terms of surface terms and an integral of the same form but with a larger power of r in the denominator which should converge more rapidly than the original integral as $r \to \infty$. Repeating the above procedure n times we obtain the following asymptotic series for $I^1_{L-1}(R)$:

$$I^1_{L-1}(R) = \left(1 + \frac{C_L}{2ipR} + \frac{C_L C_{L+1}}{(2ipR)^2} + \cdots + \frac{C_L C_{L+1} \cdots C_{L+n-2}}{(2ipR)^{n-1}}\right) \frac{\sigma_E}{2ipR} S^1_{KK'}(R)$$
$$+ \left(\frac{1}{L+1} + \frac{C_L}{(L+2)(2ipR)} + \cdots + \frac{C_L C_{L+1} \cdots C_{L+n-2}}{(L+n)(2ipR)^{n-1}}\right) \frac{B}{2ipR} S^2_{KK'}(R)$$
$$+ \frac{1}{(2ipR)^n} C_L C_{L+1} + \cdots C_{L+n-1} I^1_{L+n-1}(R) \,. \tag{32}$$

A suitable choice of n results in a negligible contribution of the last term in the above equation except for cases of large angular momentum partial waves for which the electron wave functions do not penetrate the nucleus appreciably. In these cases, however, the analytic expressions for the point radial integrals given by Reynolds, Onley, and Biedenharn[7] can be used. Thus, by using the asymptotic series given above, we can confine all numerical integration to the nuclear interior and the remaining contributions from R to ∞ are given in terms of the electron wave functions at the nuclear surface just as in the case for spherically symmetric charge scattering. Note that the recursion relation we are using here is a special case of a more general relationship involving relativistic Coulomb radial integrals with energy transfer to the nucleus.[8]

Plane-wave Born approximation

The PWBA as applied to elastic electron scattering is discussed extensively in many sources (see Ref. 4, for example) and here we will only state the results in terms of our notation so that comparison of results between DWBA and PWBA will be facilitated. In PWBA, the elastic electron scattering cross section from a fixed target can be written as

$$\frac{d\sigma(\theta)}{d\Omega} = \frac{4\pi\alpha^2}{p^2(2J+1)} \left[\sum_{L=\text{even}} |F^C_L(q)|^2 V_L(\theta) + \sum_{L=\text{odd}} |F^{TM}_L(q)|^2 V_T(\theta) \right], \tag{33}$$

where

$$V_L(\theta) = \frac{2p^2}{q^4}\left[p^2(1+\cos\theta) + 2m_0^2\right],$$

$$V_T(\theta) = \frac{p^4}{q^4}(3 - \cos\theta),$$

and the momentum transfer $q = 2p\sin\frac{1}{2}\theta$. The form factors are defined in terms of the charge and current distribution as

$$F^C_L(q) = \int_0^\infty \rho_L(r) j_L(qr) r^2 dr$$

and

$$F^{TM}_L(q) = \int_0^\infty j_{L,L}(r) j_L(qr) r^2 dr \,.$$

From the above we can immediately see that as $\theta \to 180°$ that $V_L/V_T \cong m_0^2/p^2$ and that magnetic scattering for high-energy electrons should dominate at backward angles. Also if we take the so-called high-energy limit, $m_0^2/p^2 \to 0$, we can rewrite Eq. (33) in a more familiar form:

$$\left.\frac{d\sigma(\theta)}{d\Omega}\right|_{m_0/p \to 0} = \frac{4\pi\alpha^2\cos^2\frac{1}{2}\theta}{E^2(2J+1)\sin^4\frac{1}{2}\theta} \times \sum_{L=\text{even}} |F^C_L(q)|^2 + (\tfrac{1}{2} + \tan^2\tfrac{1}{2}\theta) \times \sum_{L=\text{odd}} |F^{TM}_L(q)|^2 . \tag{34}$$

Charge and current distributions

In order to investigate the nuclear magnetization distribution it is in general necessary to subtract the charge scattering, thus requiring a parametrization of the nuclear charge distribution. We are primarily interested in nearly spherical medium and heavy nuclei and the ground-state charge distribution of such nuclei is well described (up to some maximum moment transfer) by a Fermi distribution. Thus we choose

$$\rho_0(r) = \frac{\rho_0}{1 + \exp[(r-c)/(t/4\ln 3)]} \,, \tag{35}$$

where the half-density radius c and skin thickness t are fitted to forward-angle elastic electron scattering where magnetic scattering contributions are negligible. Our formalism given above includes the possibility of calculating the higher electric multipole scattering, but as we have not

yet included this in our computer codes, we restrict our attention in this paper to nearly spherical nuclei where the higher electric multipole contributions can be neglected.

It is also necessary to parametrize the magnetization distribution and since only unpaired nucleons (viewed if you wish as quasiparticles) can contribute to the magnetization distribution, we will use the single-particle model for that purpose. The operators for the orbital current and spin magnetization distribution due to a single unpaired nucleon are

$$j_0^{0p} = \frac{-ie}{2M} g_l [\delta(\vec{r} - \vec{r}_i)\vec{\nabla}_{r_i}]_{\text{sym.}}$$

and

$$\vec{\mu}_s^{0p} = \frac{e}{2M}\gamma_i \delta(\vec{r} - \vec{r}_i)\vec{\sigma}_i ,$$

where

$$g_l = \begin{cases} 1 \text{ proton} \\ 0 \text{ neutron} \end{cases}, \quad \gamma_i = \frac{g_s}{2} = \begin{cases} 2.79 \text{ proton} \\ -1.91 \text{ neutron} \end{cases},$$

and M is the nucleon mass.

The single-particle wave function is given explicitly by

$$\psi^m_{nlj}(\vec{r}) = R_{nl}(r) \sum_{m_l, m_s} C^{l}_{m_l\, m_s^{\frac{1}{2}}\, m}^{j}\, Y_l^{m_l}(\hat{r})\chi^{m_s}_{\frac{1}{2}} .$$

For simplicity we use harmonic-oscillator wave functions for $R_{nl}(r)$ which are given by

$$R_{nl}(r) = \left(\frac{2\Gamma(n+l+3/2)}{n!\, b^3}\right)^{1/2} \frac{1}{\Gamma(l+3/2)} \left(\frac{r}{b}\right)^l e^{-r^2/2b^2} \times {}_1F_1(-n, l+\tfrac{3}{2}; r^2/b^2) ,$$

where the range parameter $b = (\hbar/M\omega)^{1/2}$ is chosen to agree with the experimentally determined rms charge radius of the nucleus.

The radial parts of the nuclear current and spin magnetization densities of Eqs. (21) and (22) are given by

$$j_{L,L}(r) = -\int \langle nlj \| \vec{Y}^M_{L,L} \cdot \vec{j}_0^{0p} \| nlj \rangle \, d\Omega$$

and

$$\mu_{L,L\pm1}(r) = \int \langle nlj \| \vec{Y}^M_{L,L\pm1} \cdot \vec{\mu}_s^{0p} \| nlj \rangle d\Omega ,$$

where we use the reduced matrix element convention of Edmonds.[9] The operators $\vec{Y}^M_{L,L} \cdot \vec{j}_0^{0p}$ and $\vec{Y}^M_{L,L\pm1} \cdot \vec{\mu}^{0p}$ can be written

$$\vec{Y}^M_{L,L} \cdot \vec{j}_0^{0p} = \frac{ie}{M}\left(\frac{2L+1}{L+1}\right)^{1/2} g_l \frac{\delta(\vec{r} - \vec{r}_i)}{r} \vec{Y}^M_{L,L-1} \cdot \vec{l} \qquad (36)$$

and

$$Y^M_{L,L\pm1} \cdot \vec{\mu}_s^{0p} = \frac{e}{2M}\gamma_i \delta(\vec{r} - \vec{r}_i)\vec{Y}^M_{L,L\pm1} \cdot \vec{\sigma} , \qquad (37)$$

where in Eq. (36), $\vec{l} = -i\vec{r} \times \vec{\nabla}$ and we have used the fact that symmetrization only produces a factor of 2. Using the reduced matrix elements of $\vec{Y}^M_{L,L-1} \cdot \vec{l}$ and $\vec{Y}^M_{L,L\pm1} \cdot \vec{\sigma}$ between single-particle states as given by Willey[10] we obtain:

$$j^0_{L,L}(r) = \frac{ie}{M}(-1)^{j-1/2} g_l (2L+1)(2l+1)(2j+1) \times \left(\frac{(2L-1)l(l+1)(2l+1)}{4\pi(L+1)}\right)^{1/2} \begin{pmatrix} l & j & \frac{1}{2} \\ j & l & L \end{pmatrix} \times \begin{pmatrix} L-1 & 1 & L \\ l & l & l \end{pmatrix} \begin{pmatrix} l & L-1 & l \\ 0 & 0 & 0 \end{pmatrix} \frac{R_{nl}^2(r)}{r} \qquad (38)$$

and

$$\mu_{L,L'}(r) = \frac{e}{2M}(-1)^l (2l+1)(2j+1) \times \left(\frac{6(2L+1)(2L'+1)}{4\pi}\right)^{1/2} \begin{pmatrix} l & l & L' \\ \frac{1}{2} & \frac{1}{2} & 1 \\ j & j & L \end{pmatrix} \times \begin{pmatrix} l & L' & l \\ 0 & 0 & 0 \end{pmatrix} R_{nl}^2(r) . \qquad (39)$$

Before applying the formalism developed above to some particular examples let us examine some general properties of magnetic multipole moments in a single-particle model. A nucleus with spin J can have magnetic moments $M1$, $M3$, ... ML where $L = 2J$. We can see immediately from Eq. (38) that for $j = l + \frac{1}{2}$ orbitals, the orbital current for $L = 2j$ vanishes due to the $6j$ symbol

$$\begin{pmatrix} j-\frac{1}{2} & j & \frac{1}{2} \\ j & j-\frac{1}{2} & 2j \end{pmatrix} .$$

Of course, the orbital current vanishes for all L for neutron orbitals. Thus, in both of these cases, the single-particle model predicts that only the intrinsic magnetization contributes to the magnetic scattering of electrons. As noted by Donnelly and Walecka,[3] another case of great interest is orbitals with the highest-j values in an oscillator shell. The 1p-1h mixtures into such an orbital cannot contribute to the $L = 2j$ magnetization distribution, and 2p-2h admixtures should be small since 2p-2h states are far away in energy; thus such orbitals should be quite well described by the single-particle model.

RESULTS

We have used the formalism given above to analyze elastic electron scattering over a range

of energies from various nuclei. As there are not very many data available on the medium and heavy nuclei, we have primarily undertaken the task of examining the possibilities of using electron scattering to measure the magnetization distribution in medium and heavy nuclei. In those cases where experimental data are available, we have anaylzed it in terms of our model.

Since these calculations involve extensive numerical computation it is important to compare the results in certain limits with analytic results. We do this by setting $Z\alpha$ in our computer codes to a small value ($Z\alpha = 10^{-3}$) and then performing the complete distorted-wave calculation. This essentially turns off the static Coulomb potential and hence results in no distortion of the electron wave functions. The results obtained this way agree with the plane-wave Born approximation over the complete angular range to within 1% except at the Born zeros. This result in addition to numerous internal checks on series conversion provides an excellent check on the over-all calculational procedure.

Before discussing the size of the magnetic contributions to elastic electron scattering in a few explicit cases we should examine other possible contributions. Charge scattering from the spherically symmetric part of the nuclear charge distribution must of course be included, but as noted previously, charge elastic scattering can also occur from electric quadrupole and higher even multipole moments. We have not included such contributions in our computer codes and as long as we avoid the strongly deformed nuclei we expect small contributions from the higher electric multipole moments. This is based on our experience with 200-MeV electron scattering from ^{165}Ho which over a wide angular range contains roughly equal contributions from charge and electric quadrupole scattering.[11] The nucleus ^{165}Ho is strongly deformed ($Q_0 = 8$ b), and since nearly spherical nuclei have quadrupole moments almost an order of magnitude less, we expect quadrupole scattering to be negligible.

As an example of elastic electron scattering from a heavy nucleus we choose ^{209}Bi which consists of an $h_{9/2}$ proton outside a ^{208}Pb core. The charge distribution of ^{209}Bi is described by a Fermi distribution with half-density radius $c = 6.73$ fm and skin thickness $t = 2.12$ fm. The $h_{9/2}$ proton is described by a harmonic-oscillator radial wave function with range parameter $b = 2.33$ fm which in a single-particle shell model would predict the experimentally determined rms radius of ^{209}Bi.

Figure 1 displays the radial dependence of the orbital current distribution and the magnetization distribution divided by r arising from this single-

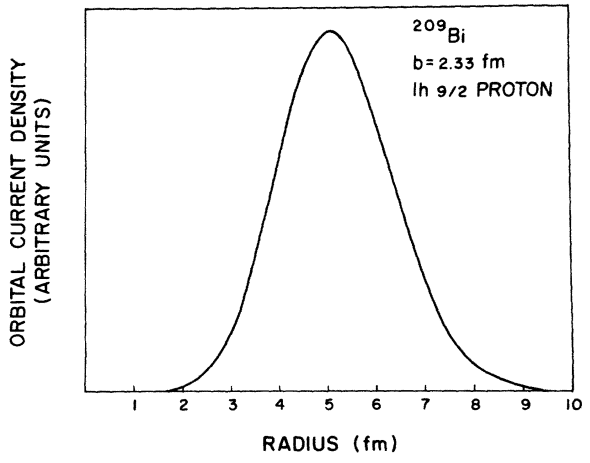

FIG. 1. The radial dependence of the orbital current density $\vec{J}_0(\vec{r})$ and the magnetization density $\vec{\mu}(\vec{r})/r$ due to the $h(\frac{9}{2}^-)$ proton of ^{209}Bi.

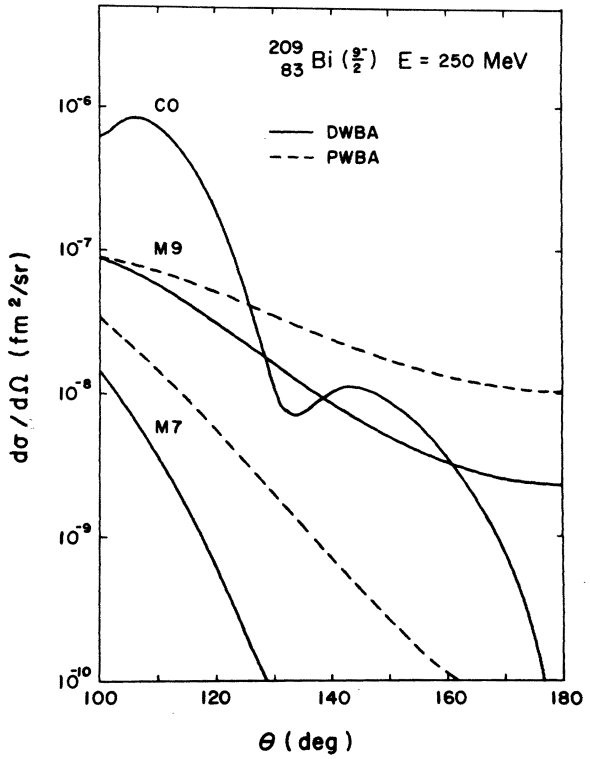

FIG. 2. The differential elastic scattering cross section of 250-MeV electrons from ^{209}Bi calculated in plane-wave Born approximation (PWBA) and distorted-wave Born approximation (DWBA) as a function of scattering angle θ. The labels $C0$, $M9$, and $M7$ refer to charge scattering and scattering from the $L = 9$ magnetic multipole and $L = 7$ magnetic multipole, respectively.

particle orbital. Note that all multipole components of the orbital distribution and the magnetization distribution divided by r have the same radial dependence. The radial dependence of the total current $\vec{j}_T(\vec{r}) = \vec{j}_0(r) + \vec{\nabla} \times \vec{\mu}$ is however not given by this curve as may be seen from Eq. (25).

Figure 2 shows the elastic electron scattering cross section of 250-MeV electrons from the charge distribution and the $L = 7$ and 9 magnetization distributions for ^{209}Bi. The dashed and solid curves are the PWBA and DWBA magnetic scattering cross sections, respectively. Clearly the magnetization cross section is affected appreciably by Coulomb distortion for such a heavy nucleus. The magnitudes of the magnetic multipole scattering cross sections are taken to be those predicted by our extreme single-particle model. Since the $h_{9/2}$ orbital is a $j = l - \frac{1}{2}$ proton orbital, the contributions to the $M7$ and $M9$ moments from the orbital and spin magnetization currents enter with opposite sign. Quenching of the orbital contribution would tend to increase the magnetic scattering cross section, so these curves may well be lower bounds on the magnetization contribution. The dominant magnetic contribution is $M9$ and is clearly measurable near 180°, and furthermore should be observable around 130 to 140° for 250-MeV electron scattering.

Figure 3 shows the charge and magnetic scattering of 183-MeV electrons calculated in PWBA and DWBA from ^{51}V. We describe the spherically symmetric charge distribution of ^{51}V by a Fermi distribution with half-density radius $c = 3.95$ fm and skin thickness $t = 2.24$ fm. The nucleus ^{51}V can be described in a simple shell model as three $f_{7/2}$ protons outside a ^{48}Ca core. We attribute all the magnetic properties of ^{51}V to a single unpaired proton orbital described by a harmonic-oscillator wave function with range parameter $b = 2.01$ fm. Again, as in the case of ^{209}Bi, the highest allowed magnetic multipole is dominant and according to the extreme single-particle model exceeds charge scattering from approximately 130° on back to 180°. Note that distortion even here is appreciable except for near a diffraction maxima where a shift in angle has minimal effect. The typical marching pattern of the various multipoles can be seen in this figure.

Figure 4 shows the elastic scattering of 200-MeV electrons from ^{209}Bi where again the magnetic

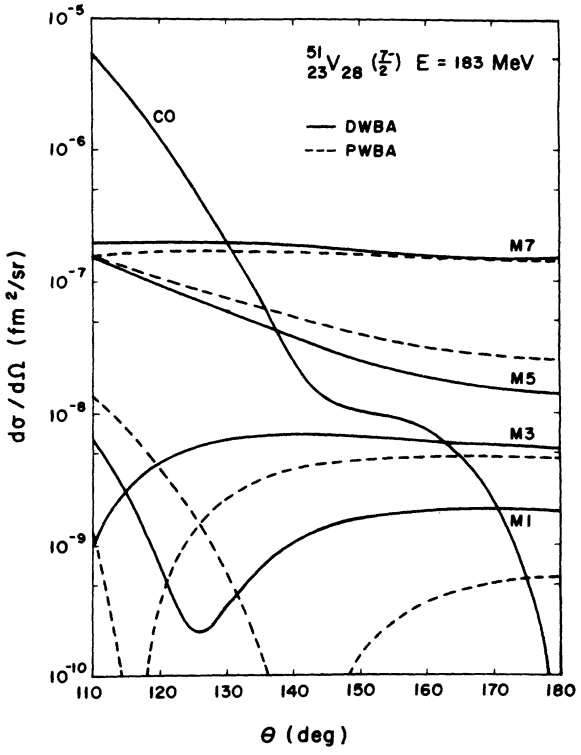

FIG. 3. The differential elastic scattering cross section of 183-MeV electrons from ^{51}V in PWBA and DWBA as a function of scattering angle θ. The labels $C0$ and $M1$–$M7$ refer to charge and magnetic multipole scattering, respectively.

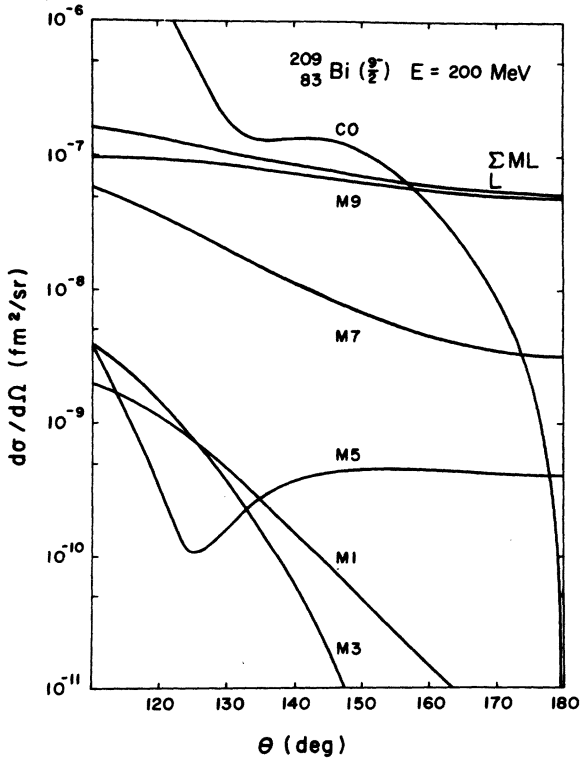

FIG. 4. The differential charge and magnetic multipole elastic scattering cross sections of 200-MeV electrons from ^{209}Bi as a function of scattering angle θ.

terms are those predicted by the extreme single-particle model which for magnetic dipole ($M1$) are referred to by the term Schmidt value. Again the highest multipole dominates, but is only easily observable according to the single-particle model at extreme backward angles. This figure also displays the dramatic minimum of charge scattering at 180°. By increasing the electron energy to 300 MeV the charge and $M9$ scattering can be shifted relative to each other and we obtain the results shown in Fig. 5. Note that at this energy we are near a minimum in the $M9$ scattering at backward angles, but it should be possible to measure the $M9$ scattering from 100 to 110° and from 130 to 140°.

The above results indicate that magnetic scattering, primarily from the maximally allowed multipole, should be easily measured as a function of energy E and hence momentum transfer at 180°. Furthermore, if the single-particle model predicts the correct magnitude of the magnetization current, magnetic scattering can be observed at normal angles with judicious choices of the incident electron energies.

A recent experiment performed at Tohoku by Peterson *et al.*[12] indicated the presence of transverse terms at 90° in the elastic cross section of 250-MeV electrons on ^{51}V. We calculated the charge and magnetic scattering of 250-MeV electrons from ^{51}V using the parameters given above and we find the fit to experimental data shown in Fig. 6. In order to fit the data point at 90° we need to reduce the magnetic scattering due to the $M7$ distribution (the lower moments have negligible contribution in this region) by a factor of 0.40. Based on this one data point, we estimate the $M7$ moment of ^{51}V to be $(-23b^6)\mu_N$ as compared to $(-37b^6)\mu_N$ predicted by the single-particle model. This value is not unreasonable considering that there are three protons outside the ^{48}Ca core. We would strongly encourage additional experiments on ^{51}V at larger angles and other energies in order to extract the radial shape and magnitude of the $M7$ magnetization distribution.

Another nucleus for which extensive investigations of magnetic electron scattering have been carried out is ^{27}Al. Unfortunately the charge distribution has not been adequately examined. The rms radius of ^{27}Al was determined by a low-q experiment some years ago to be 3.01 fm.[13] We

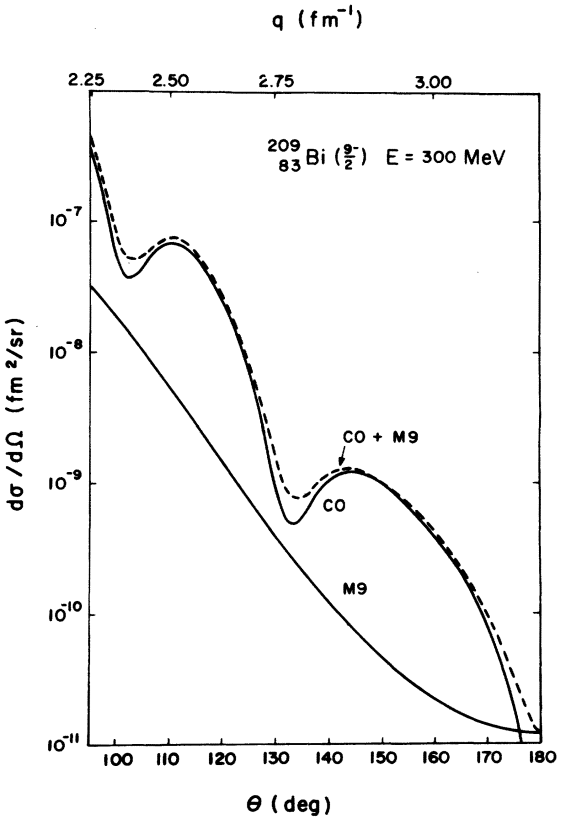

FIG. 5. The differential charge and $L=9$ magnetic multipole elastic scattering cross sections of 300-MeV electrons from ^{209}Bi as a function of scattering angle θ and momentum transfer q.

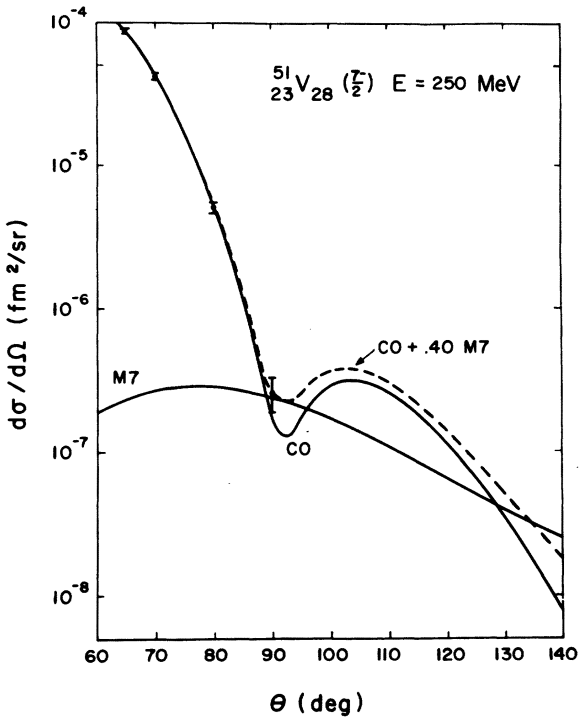

FIG. 6. The differential elastic scattering cross section of 250-MeV electrons from ^{51}V as a function of scattering angle θ and momentum transfer q. The experimental points are those of Peterson *et al.* (Ref. 12).

attempted to fit the 500-MeV data of Li *et al.*[14] by using a Fermi distribution for $\rho_0(r)$ with half-density radius c and skin thickness t chosen to fit the experimentally determined rms radius. This, however, leaves considerable latitude in choosing c and t. We attributed the magnetic properties of ^{27}Al to a $d_{5/2}$ hole in a ^{28}Si core. The range parameter for this orbital is $b = 1.81$ fm which would reproduce the experimental determined rms radius in a single-particle model. Our fit to the data is shown in Fig. 7. We were unable to obtain a better fit by varying c and t while keeping the rms radius constant. The magnetic contribution seems reasonable in view of the 180° scattering experiment of Lapikas, Dieperink, and Box[2] which determined the $M5$ moment of ^{27}Al to be $[(6.4 \pm 0.7)b^4]\mu_N$. We have used the single-particle value of $(10.5b^4)\mu_N$ in this figure. However, the charge scattering at these angles probably contains some higher electric multipole contributions since ^{27}Al is believed to be rather deformed. We recommend some moderate-energy elastic scattering experiments on ^{27}Al at forward angles in order to determine the charge distribution more completely. This case illustrates the difficulty in determining magnetic scattering when the charge distribution is not well known.

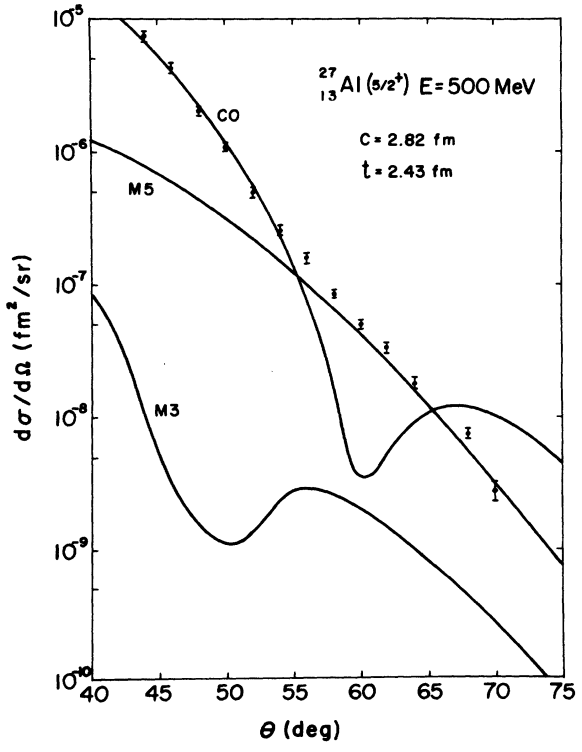

FIG. 7. The differential elastic scattering cross section of 500-MeV electrons from ^{27}Al as a function of scattering angle θ. The experimental points are taken from Ref. 14.

The examples given above indicate that magnetic elastic electron scattering should be observable in the medium and heavy odd-A nuclei at normal scattering angles at particular values of the electron energies, and in general at 180°. The procedure to be followed at normal scattering angles is to determine the nuclear charge distribution by performing experiments over a wide range of momentum transfer at forward angles where magnetic scattering is negligible; then to do experiments at scattering angles as large as possible. At these large scattering angles the charge scattering can be subtracted out by the phase-shift calculation leaving the magnetic scattering.

In summary, we encourage further elastic electron scattering experiments at relatively large angles in addition to 180° experiments with the goal of extracting the magnetization distribution of the medium and heavy odd-A nuclei. The $L = 2J$th magnetization distribution should be particularly easy to determine and within a single-particle model is in many cases essentially the $(2J-1)$th moment of the square of a single-particle wave function and may be of considerable interest for odd neutron nuclei. We also note that since the orbital and spin terms enter the magnetization in quite different ways that elastic electron scattering with its variable momentum transfer may be capable of investigating quenching of the magnetic moments and the effects of "exchange currents" in more detail than other methods.

We wish to thank Professor D. S. Onley for many useful ideas and suggestions for carrying out this work.

APPENDIX

The normalized solutions to the radial Dirac-Coulomb equations [Eqs. (4) in the text] for the point Coulomb potential $V(r) = -\alpha Z/r$ are

$$\begin{pmatrix} f_\kappa^{R,I}(r) \\ g_\kappa^{R,I}(r) \end{pmatrix} = \begin{pmatrix} -\left(\frac{(E-m_0)}{(E+m_0)}\right)^{1/2} \mathrm{Im}[V_{\pm\gamma}(pr)] \\ \mathrm{Re}[V_{\pm\gamma}(pr)] \end{pmatrix}, \quad \text{(A1)}$$

where

$$V_\gamma(pr) = 2e^{\pi y/2} \frac{|\Gamma(\gamma+iy)|}{\Gamma(2\gamma+1)} (2pr)^{\gamma-1}(\gamma+iy) \times e^{i[\eta_\kappa(\gamma)-pr]}\, {}_1F_1(1+\gamma+iy;\, 2\gamma+1;\, 2ipr). \quad \text{(A2)}$$

The phases

$$\eta_\kappa(\gamma) = -\tfrac{1}{2}\pi\left(\frac{1+S_\kappa}{2}\right) - \tfrac{1}{2}\arctan\left(\frac{y(\kappa+\gamma m_0/E)}{\kappa\gamma - y^2 m_0/E}\right). \tag{A3}$$

The labels R and I refer to regular and irregular solutions which are given by the upper and lower signs of γ, respectively. These phases are related to the point Coulomb phases given in Eq. (12) by

$$\delta_\kappa^{\mathrm{R}}(\gamma) = \eta_\kappa(\gamma) - \tfrac{1}{2}\pi\gamma - \arg\Gamma(\gamma+iy) + \frac{l+1}{2}\pi \tag{A4}$$

and

$$\delta_\kappa^{\mathrm{I}}(\gamma) = \delta_\kappa^{\mathrm{R}}(-\gamma).$$

The asymptotic forms of these functions are

$$f_\kappa^{\mathrm{R,I}}(r) \to -\left(\frac{E-m_0}{E+m_0}\right)^{1/2} \times \frac{\sin[pr + y\ln 2pr - \frac{1}{2}(l+1)\pi + \delta_\kappa^{\mathrm{R,I}}]}{pr},$$

$$g_\kappa^{\mathrm{R,I}}(r) \to \frac{\cos[pr + y\ln 2pr - \frac{1}{2}(l+1)\pi + \delta_\kappa^{\mathrm{R,I}}]}{pr}. \tag{A5}$$

To calculate these functions numerically we write

$$V_\gamma(pr) = \frac{e^{\pi y/2} e^{i\eta_\kappa(\gamma)}}{2pr} \times [(\gamma+iy)U_\gamma(pr) + i|\gamma+iy|\,U_{\gamma+1}(pr)], \tag{A6}$$

where

$$U_\gamma(pr) = \frac{|\Gamma(\gamma+iy)|}{\Gamma(2\gamma)}(2pr)^\gamma e^{-ipr}\,{}_1F_1(\gamma+iy;2\gamma;2ipr). \tag{A7}$$

We calculate $U_\gamma(pr)$ by a series expansion about the origin for $pr \le 15$ and an asymptotic expansion for $pr > 15$. The power series for $U_\gamma(pr)$ about the origin is

$$U_\gamma(pr) = \frac{|\Gamma(\gamma+iy)|}{\Gamma(2\gamma)}(2pr)^\gamma \sum_{n=0}^{\infty} a_n (pr)^n, \tag{A8}$$

where $a_0 = 1$, $a_1 = -y/\gamma$, and

$$a_n = -\frac{(2ya_{n-1} + a_{n-2})}{n(n+2\gamma-1)}, \quad n \ge 2.$$

The asymptotic series for $U_\gamma(pr)$ is

$$U_\gamma(pr) = 2\,\mathrm{Re}\left(\frac{|\Gamma(\gamma+iy)|}{\Gamma(\gamma+iy)} e^{ipr} e^{-\pi/2(y+\gamma)} e^{iy\ln 2pr} \times \sum_n b_n (pr)^{-n}\right), \tag{A9}$$

where

$$b_0 = 1, \quad b_1 = \frac{(\gamma-iy)(1-\gamma-iy)}{2i}$$

and

$$b_n = \frac{(\gamma - iy + n - 1)(n - \gamma - iy)}{2in} b_{n-1}; \quad n \ge 2.$$

The power series of Eq. (A8) converges more rapidly for large positive values of γ while the asymptotic series of Eq. (A9) converges more rapidly for large positive or negative values of γ. The following recursion relation satisfied by $U_\gamma(pr)$ can be used to choose the value of γ to obtain the most rapid convergence of the particular series being used:

$$U_\gamma(pr) = \frac{1}{|\gamma-1+iy|(\gamma-2)} \times \left(\frac{2(\gamma-3/2)}{pr}[(\gamma-1)(\gamma-2) - ypr]\,U_{\gamma-1}(pr) - |\gamma-2+iy|(\gamma-1)U_{\gamma-2}(pr)\right). \tag{A10}$$

The function $V_{-\gamma}(pr)$ which is needed for the irregular point Coulomb solution is calculated in a similar fashion by changing the sign of γ everywhere and using the recursion relation in the opposite direction. This calculational method and the associated computer programs were furnished to us by Dieter Drechsel.

*Supported in part by the U. S. Army Research Office (Durham).

[1]T. A. Griffy and D. U. L. Yu, Phys. Rev. 139, B880 (1965).
[2]L. Lapikas, A. E. L. Dieperink, and G. Box, Nucl. Phys. A203, 609 (1973).
[3]T. W. Donnelly and J. D. Walecka, Nucl. Phys. A201, 81 (1973).
[4]H. Überall, *Electron Scattering from Complex Nuclei* (Academic, New York, 1971), Part A.
[5]G. A. Peterson and W. C. Barber, Phys. Rev. 128, 812 (1962).
[6]D. R. Yennie, D. G. Ravenhall, and R. N. Wilson, Phys. Rev. 95, 500 (1954).
[7]J. T. Reynolds, D. S. Onley, and L. C. Biedenharn, J. Math. Phys. 5, 411 (1964).
[8]D. S. Onley, *Nuclear Structure Studies Using Electron Scattering and Photoreaction* (Tohoku University, Sendai, Japan, 1972).
[9]A. R. Edmonds, *Angular Momentum in Quantum Mechanics* (Princeton U. P., Princeton, New Jersey, 1957).
[10]R. S. Willey, Nucl. Phys. 40, 529 (1963).
[11]L. E. Wright, Nucl. Phys. A135, 139 (1969).
[12]G. A. Peterson, K. Hosoyama, M. Nagao, A. Nakada, and Y. Torizuka, Phys. Rev. C 7, 1028 (1973).
[13]H. A. Bentz, M. Loewenhaupt, and H. Theissen, Z. Phys. 231, 434 (1970).
[14]G. C. Li, I. Sick, J. D. Walecka, and G. E. Walker, Phys. Lett. 32B, 317 (1970).